JOURNAL OF CATALYSIS **177,** 137–146 (1998)
ARTICLE NO. CA982092

# Spectroscopic and Microscopic Characterization of Iron- and/or Manganese-Promoted Sulfated Zirconia

Markus Scheithauer,* Eric Bosch,* Uwe A. Schubert,* Helmut Knözinger,*,[1] Tsz-Keung Cheung,† Friederike C. Jentoft,†,[2] Bruce C. Gates,† and Bernd Tesche‡

*Institut für Physikalische Chemie, Universität München, Sophienstraße 11, D-80333 Munich, Germany; †Department of Chemical Engineering and Materials Science, University of California, Davis, California 95616; and ‡Max-Planck-Institut für Kohlenforschung, Kaiser Wilhelm Platz 1 , Mülheim a. Ruhr D-45470, Germany

Received January 5, 1998; revised March 18, 1998; accepted March 19, 1998

**The structures of iron-promoted sulfated zirconia (FSZ), manganese-promoted sulfated zirconia (MSZ) and iron- and manganese-promoted sulfated zirconia (FMSZ) were investigated by ultraviolet-visible (UV-vis) diffuse reflectance, ESR, laser Raman, and X-ray photoelectron (XP) spectroscopies and by transmission electron microscopy with energy dispersive X-ray microanalysis. The bulk structure of tetragonal zirconia and the surface sulfate structure of SZ remained virtually unchanged when the promoters were added to SZ, as shown by laser Raman spectroscopy. The UV-vis spectra show that iron was present in aggregated structures and not as atomically isolated species. The Raman spectra identify these dispersed structures as $Fe_2O_3$, and the electron micrographs confirm the presence of particulate structures on the surfaces of FSZ and FMSZ, but not SZ and MSZ. The XP spectra provide confirming evidence of $Fe^{3+}$, consistent with the presence of $Fe_2O_3$, and the ESR spectra show the presence of $Fe^{3+}$ ions in a broad distribution of coordination environments. The evidence of particulate $Fe_2O_3$ is in agreement with the results of J. E. Tabora and R. J. Davis (*J. Chem. Soc. Faraday Trans.* 91, 1825 (1995)), whose Fe-edge extended X-ray absorption fine structure spectra showed the lack of Fe–Zr and Fe–Fe contributions, consistent with particulate iron oxide clusters and inconsistent with iron in the bulk zirconia. Manganese in MSZ and FMSZ is identified by the ESR spectra as $Mn^{2+}$, with the resolved hyperfine structure indicating that part of the $Mn^{2+}$ ions were highly dispersed in still unknown locations in FMSZ. The results are not sufficient to establish the nature of the promoter effects or to resolve the nature of the interactions between Mn and Fe indicated by catalyst performance data (F. C. Lange *et al., Catal. Lett.* 41, 95 (1996)), showing that FMSZ is much more active than either FSZ or MSZ for isomerization of *n*-butane.** 

## INTRODUCTION

Sulfated zirconia (SZ) and related acidic catalysts have drawn attention recently because of their high activities for conversion of light alkanes (1–3). The catalysts incorporate surface sulfate groups, and, consistent with the composition of these groups, X-ray photoelectron spectroscopy indicated that the oxidation state of S in SZ was +6 (1). X-ray diffraction, Raman spectroscopy, and X-ray absorption spectroscopy provided evidence that the bulk structure of the zirconia in SZ is predominantly tetragonal, and it has been suggested that the high-surface-area tetragonal phase is necessary for high catalytic activity of SZ (1, 4). However, it has recently been shown that high-surface-area monoclinic SZ can also be prepared, giving catalysts with activities comparable to those containing tetragonal zirconia (5).

Promoted SZ, exemplified by Fe- and Mn-promoted SZ (FMSZ), was reported (6) to be 2–3 orders of magnitude more active than SZ for *n*-butane isomerization. Only little has been reported characterizing the structures of promoted catalysts such as FMSZ. Consistent with results characterizing SZ, infrared and Raman spectra of FMSZ gave evidence of surface sulfate groups (7–9). On the basis of a lack of Fe–Fe and Fe–Zr contributions in the extended X-ray absorption fine structure (EXAFS) spectrum of FMSZ, Tabora and Davis (10) concluded that iron was not present in the zirconia and suggested that it was, instead, present in small supported iron oxide clusters. High-resolution transmission electron microscopy of FMSZ reported by Benaissa *et al.* (11), however, gave no evidence of supported metal oxide clusters, and Benaissa *et al.* hypothesized that iron and manganese were dispersed at the atomic level on the zirconia surface.

Because the reported structural characterizations of FMSZ are fragmentary and inconsistent, we attempted to use a set of complementary physical methods for a structural investigation of a family of sulfated zirconia samples, including FMSZ, unpromoted SZ, Mn-promoted SZ (MSZ), and Fe-promoted SZ (FSZ). We report results of characterization by UV-visible diffuse reflectance spectroscopy (UV-vis), ESR, laser Raman, and X-ray photoelectron

[1] To whom correspondence should be addressed.
[2] Current address: Fritz-Haber-Institut der Max-Planck-Gesellschaft, Faradayweg 4-6, Berlin 14195, Germany.



0021-9517/98 $25.00

(XP) spectroscopies and transmission electron microscopy (TEM). The results presented here complement catalytic data (12), showing that iron and manganese used separately are less effective as promoters of the SZ catalyst for *n*-butane isomerization than a combination of the two.

The new results provide information about the nature of the structures containing the promoters in the catalysts but they still leave open the question of how the promoters function to increase the catalytic activity.

## EXPERIMENTAL

### *Materials and Catalyst Preparation*

Details of the preparations of the SZ-supported catalysts have been reported (13); only a brief summary is given here. The starting material, sulfated zirconium hydroxide (Magnesium Elektron, Inc., 3.4 wt% $SO_4^{2-}$), was impregnated with an iron(III) nitrate or manganese(II) nitrate solution at incipient wetness to give Fe-promoted sulfated zirconium hydroxide or Mn-promoted sulfated zirconium hydroxide, respectively. The zirconia promoted with both Fe and Mn was made by stepwise aqueous impregnation with iron(III) nitrate followed by manganese(II) nitrate solution. The impregnated samples were calcined at 650°C in static air and stored in glass vials. Unpromoted SZ was made by calcination of sulfated zirconium hydroxide at 650°C.

The FMSZ contained approximately 1.5 wt% Fe, 0.5 wt% Mn, and 1.8 wt% S. These values are typical of the reported FMSZ catalysts (6, 13–15). The metal and sulfur loadings of the singly promoted catalysts FSZ and MSZ were about 2 and 1.8 wt%, respectively. The BET surface areas of FMSZ, FSZ, MSZ, and SZ were 90, 80, 70, and 100 $m^2/g$, respectively. The colors of SZ, FSZ, MSZ, and FMSZ were white, light rust, gray, and rust, respectively. However, the color of FMSZ was found to be sensitive to details of the preparation method in ways that have not yet been investigated.

The sources and purities of reference materials were as follows: MnO, pure, Riedel-De Haën; $MnO_2$, 85%, Fluka; $Fe_2O_3$, purified, Riedel-De Haën; FeO, 99%, Aldrich; $FeSO_4 \cdot 7H_2O$, puriss., Merck; $Fe_2(SO_4)_3 \cdot xH_2O$, p. a., Riedel-De Haën; and $MnSO_4 \cdot 6H_2O$, p. a., Merck.

### *Transmission Electron Microscopy*

The samples were investigated with a Hitachi HF 2000 transmission electron microscope operated at 200 keV. The samples were mounted on carbon films which were placed on copper grids. The instrument was equipped with a cold field emission source of W(310) and capable of energy dispersive X-ray (EDX) analysis. The objective lens was an analytical type (+/−15° specimen tilt) with a spherical aberration coefficient of 1.2 mm, giving a point resolution of 2.3 nm and an information limit of 0.18 nm. The microscope was fitted with a Voyager 1000/S EDX system with a 68° high-angle take-off geometry, 0.037 sr collection solid angle, and an energy resolution for Mn of 140–143 eV. Spot sizes as small as about 4 nm in diameter were analyzed in the present study. EDX spectra were taken with an acquisition time of 60 s at various positions in each sample.

### *Spectroscopic Investigations*

*Ultraviolet-visible diffuse reflectance spectroscopy.* A Perkin-Elmer Lambda 15 spectrometer with a $BaSO_4$-coated integrating sphere was used. Samples were characterized at room temperature with no pretreatment. $BaSO_4$ was used as the reference material. The sample thickness was 5 mm. The spectral resolution was 2 nm. Data were recorded for the catalyst samples and for the reference materials MnO, $MnO_2$, $Fe_2O_3$, FeO, $FeSO_4 \cdot 7H_2O$, $Fe_2(SO_4)_3 \cdot xH_2O$, and $MnSO_4 \cdot 6H_2O$. Spectra were plotted as absorbance $(1 - R_\infty)$ as a function of wavelength, where $R_\infty$ is the reflectance at infinite sample thickness.

*ESR spectroscopy.* Measurements were made with a Varian E-Line (E9) spectrometer equipped with a TE104-mode double cavity. The spectra characterizing each sample were recorded in the X-band at room temperature with a microwave power of 10 mW; $Mn^{2+}$ in MgO was used as the reference material. To examine the effect of vacuum pretreatment followed by introduction of oxygen, the Mn-containing sample was held under vacuum for 2 h at 200°C before measurements were begun. Subsequent measurements were done with no pretreatment of the sample.

*Laser Raman spectroscopy.* Raman spectra were recorded with a Dilor (OMARS 89 triple monochromator) spectrometer, equipped with a thermoelectrically cooled charge coupled device camera (Princeton Instruments). An $Ar^+$ ion laser (model series 2020, Spectra Physics) was used, and the samples in contact with air were rotated during measurements. With no sample pretreatment, spectra were recorded with the scanning multichannel technique (16, 17) with a laser power of 30–60 mW at the sample position, an exciting wavelength of 488 nm, a slit width of 150 $\mu$m, and a scan time of 10–90 s for a single spectrum. The spectral resolution was 5 $cm^{-1}$.

*X-ray photoelectron spectroscopy.* XP spectra were recorded with a modified VSW ESCA 100 photoelectron spectrometer, equipped with a hemispherical analyzer (HA 100). For excitation, $MgK_\alpha$ (1253.6 eV) and $AlK_\alpha$ (1486.6 eV) radiation were used. The analyzer was operated in the fixed analyzer transmission mode at 22 eV pass energy. The energy resolution of the analyzer was controlled by measuring the width of the $Au4f_{7/2}$ line of a sputtered and annealed Au foil, which was found to be 1.65 eV. The X-ray gun was operated at 15 mA emission current and 12 kV acceleration voltage. Samples were pretreated under vacuum ($5 \times 10^{-8}$ mbar) at room temperature for 12 h

before measurements. The base pressure of the analyzer chamber was $1.0 \times 10^{-10}$ mbar; during data collection, the pressure was still always $<5.0 \times 10^{-8}$ mbar. To determine charging effects and the work function of each sample, each signal was referenced to the signal of the C 1s line corresponding to graphitic carbon at 284.4 eV or to Zr $3d_{3/2}$ from $ZrO_2$ at 182.2 eV (18). The signals corresponding to C 1s, Zr 3d, Fe 2p, Mn 2p, S 2p, and O 1s were analyzed.

## RESULTS

### *Electron Micrographs*

Micrographs of each of the four catalysts are compared in Fig. 1. Figure 1A shows the structure of SZ, and we infer from our X-ray data (not shown) and from Raman spectroscopy (vide infra) that the visible structure is predominantly that of tetragonal zirconia. A comparison of the survey micrographs of Figs. 1A and B shows that there was little visible effect of the added Mn promoter on the structure and morphology of the sulfated zirconia. However, the samples containing Fe (FSZ, Fig. 1C) and both Fe and Mn (FMSZ, Fig. 1D) are contrasted to the SZ by the presence of scattering centers, indicating dispersed phases on the sample surface that are associated with the presence of Fe, as can be seen more clearly in Fig. 2 at larger magnification. Typical dimensions of these supported clusters are between 1 and 2 nm.

The EDX results characterizing the FSZ and FMSZ catalysts are summarized in Figs. 3 and 4, respectively. The results shown include the analyses determined for various spots in the micrographs, as shown in the figures. The analytical results, shown only for Zr, Fe, and Mn, demonstrate the heterogeneity of the samples. For example, the EDX results characterizing FSZ (Fig. 3) show an inhomogeneous distribution of the Fe with the ratio of Fe counts to Zr counts

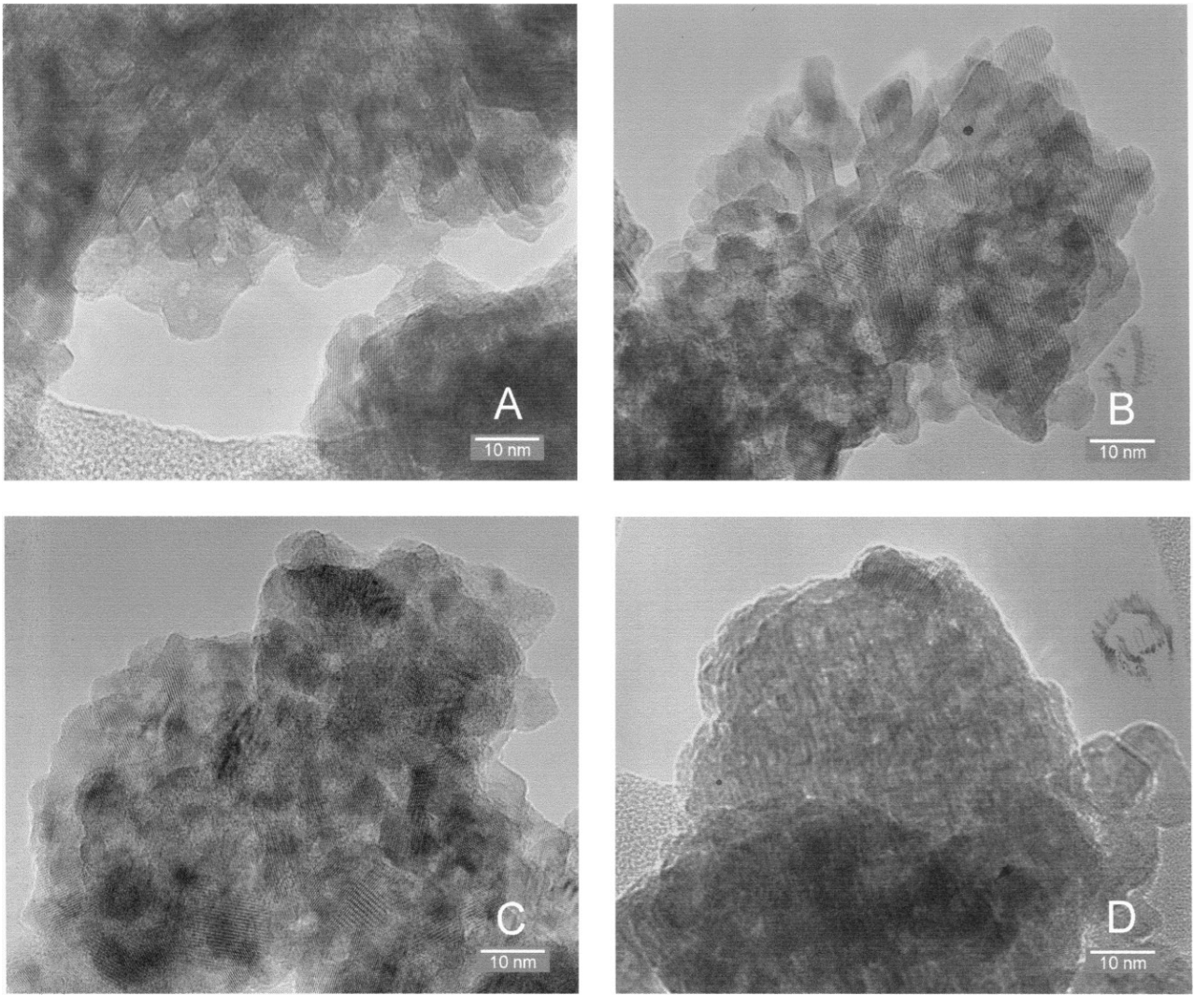


**FIG. 1.** Electron micrographs of (A) sample SZ; (B) sample MSZ; (C) sample FSZ; and (D) sample FMSZ.

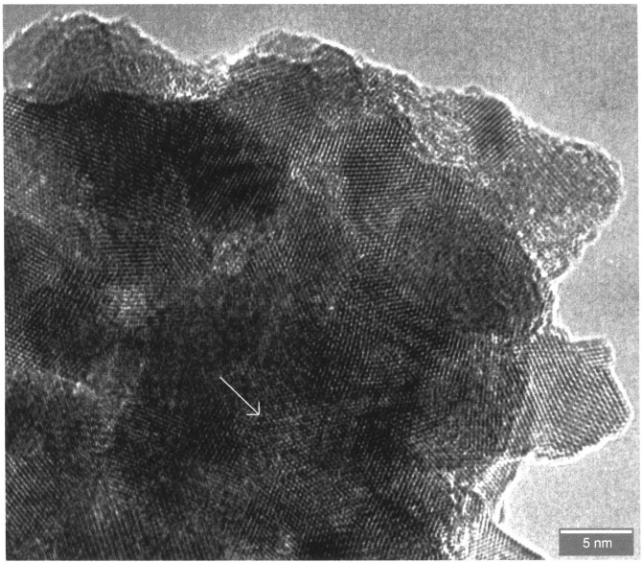


**FIG. 2.** High resolution electron micrograph of sample FSZ, part of Fig. 1C.

varying by a factor of roughly 4. The EDX results characterizing FMSZ (Fig. 4) show the presence of Zr in all but one spot examined, and, except for this one spot, the ratio of Fe counts to Zr counts varies by a factor of roughly 5. Mn was found in some of these spots but not in others (Fig. 4). The one exceptional spot was characterized by a large Fe signal and no Zr or Mn signal: this must be a particle of iron oxide; its dimension is about 50 nm. The EDX signals characterizing Mn in FMSZ are weak, consistent with the low Mn loading (0.5 wt%). The EDX data characterizing MSZ (not shown) provide more information about the Mn: Mn was consistently observed at the spots that were analyzed; and the ratio of Zr counts to Mn counts varied by a factor of roughly 2. We infer that the distribution of Mn in this sample was less heterogeneous than the distribution of Fe in FSZ and FMSZ. There is no evidence in the micrographs of MSZ for particulate Mn-containing structures.

*X-Ray Photoelectron Spectra*

All samples showed a photoelectron emission at 182.2 eV characteristic of Zr $3d_{3/2}$ and one at 530.0 eV characteristic of O 1s. These photoelectron peaks taken together are characteristic of $ZrO_2$ (18). The S 2p emission was observed at 168.7 eV and suggests the presence of $S^{6+}$ in the surface sulfate groups. Mn peaks could be detected only with a rather poor signal-to-noise ratio for MSZ; the Mn $2p_{3/2}$ peak was located at approximately 641 eV. This emission could not be detected in the spectrum characterizing FMSZ, presumably because of the low Mn concentration (0.5 wt%) in this sample.

Figure 5 shows the XP spectrum of FMSZ in the Fe 2p region. The Fe $2p_{3/2}$ and Fe $2p_{1/2}$ emissions are located at 711.1 and 724.9 eV, respectively, with a broad shake-up satellite at ~720 eV. This spectrum is clear evidence of the presence of $Fe^{3+}$ (19) and is practically identical to spectra that have been reported for $Fe_2O_3$ (20, 21).

*Raman Spectra*

The Raman spectra of SZ, FSZ, MSZ, and FMSZ are shown in Fig. 6. Each sample is characterized by peaks at 146, 270, 316, 460, and 645 $cm^{-1}$. The spectrum of SZ is characterized by the highest signal-to-noise ratio, and that of MSZ by the lowest, presumably because of its dark color. The spectra of FSZ and MSZ are very similar to that of SZ. A major band at roughly 1034 $cm^{-1}$ was observed in the spectrum of each of the SZ-supported materials; the spectrum of SZ is characterized by an additional band at about 1000 $cm^{-1}$. This band is not evident in the spectra of the other samples, presumably because of the low signal intensities.

The Raman spectra of the reference compounds FeO, $Fe_2O_3$, MnO, $MnO_2$, $FeSO_4 \cdot 7H_2O$, $Fe_2(SO_4)_3 \cdot xH_2O$, and $MnSO_4 \cdot 6H_2O$ were recorded under the same conditions applied with the catalyst samples. The spectrum of $Fe_2O_3$ is shown (Fig. 7A), because some of its spectral features (peaks at 224, 292, and 409 $cm^{-1}$) are also representative of the spectra of FMSZ and (with a much lower signal intensity) FSZ. The Raman spectrum of MSZ (spectrum d, Fig. 6) shows a rather broad shoulder near ~700 $cm^{-1}$, which is suggested to be indicative of ill-defined MnO particles because the MnO reference (Fig. 7B) shows a strong band at 657 $cm^{-1}$. This assignment is speculative. Raman spectra of other reference compounds are not shown because they are quite different from those of the SZ-supported catalysts.

*Ultraviolet-Visible Diffuse Reflectance Spectra*

The absorption spectra of SZ, FSZ, MSZ, and FMSZ are shown in Fig. 8A. These spectra are characterized by a broad step curve, and the position and the degree of steepness vary from one catalyst to another. The overall absorption is greater for the Mn-containing samples than for SZ and FSZ because of the darker color of the former. The absorption curve characterizing SZ (spectrum a, Fig. 8A) has the steepest edge. The inflection points determined from first-derivative spectra (not shown) are located at 237 and 307 nm for SZ. The low-wavelength edge at 237 nm (corresponding to 5.2 eV) is characteristic of the band gap in bulk zirconia (22). The second absorption edge, at 307 nm (4.04 eV), may be caused by impurity-induced defects. An alternative explanation is based on the fact that oxygen-to-metal charge transfer transitions are shifted to lower energy when the $O^{2-}$ ions occupy low-coordination sites, for example, at the surfaces of high-surface-area materials (23).

Additional features are superimposed on the absorption edge of SZ in the spectra of the promoted samples. A well-developed step with an inflection point at 571 nm is clearly

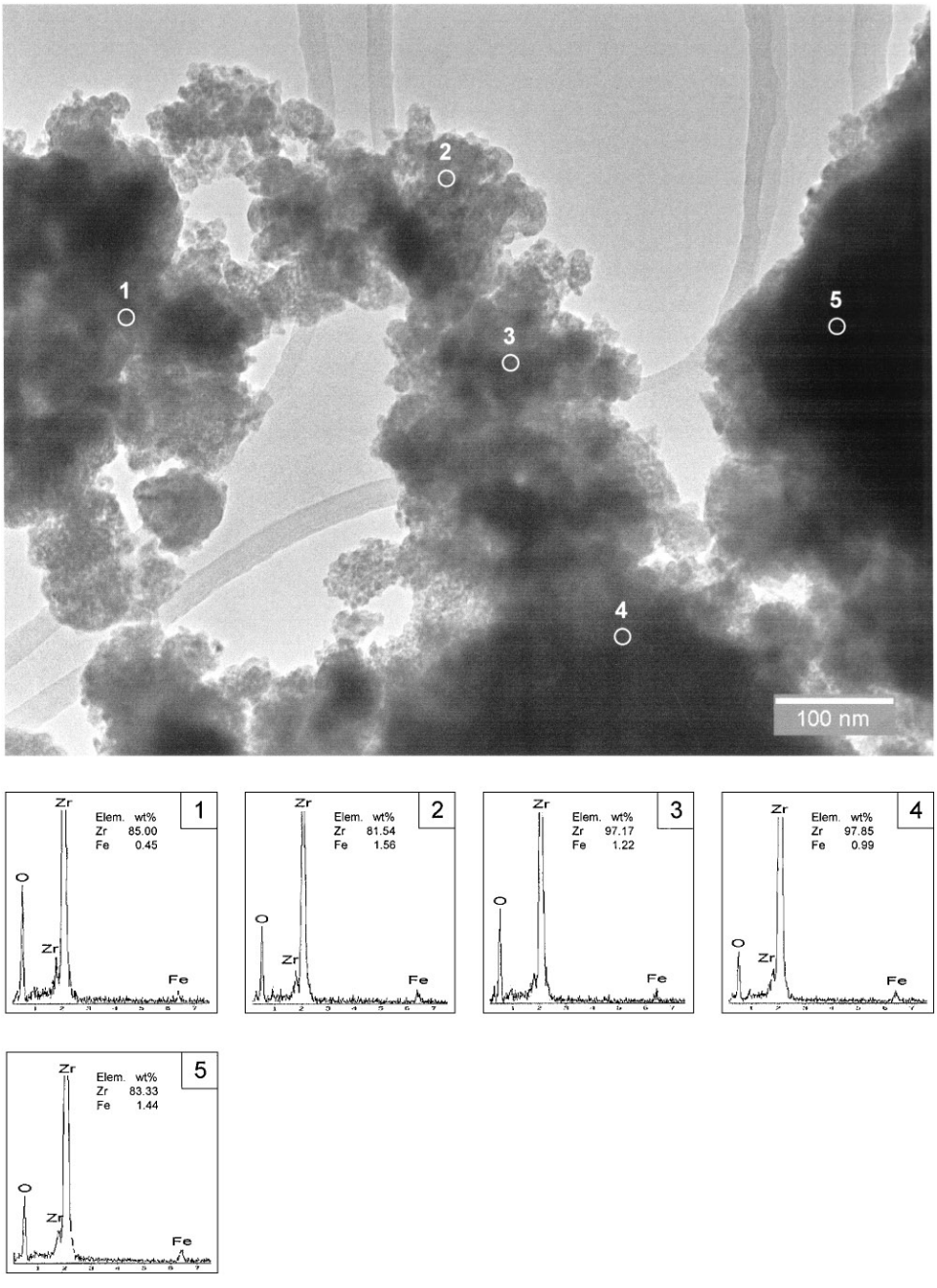


**FIG. 3.** Micrograph and EDX analysis of sample FSZ.

evident in the spectra of FSZ (spectrum b, Fig. 8A) and FMSZ (spectrum c, Fig. 8A). For comparison, the diffuse reflectance spectrum of pure $Fe_2O_3$ is shown in Fig. 8B. This spectrum is very similar to that reported (24). It has a steep edge with an inflection point at 587 nm and a strong, almost constant, absorption at lower wavelengths (higher energies). This strong absorption causes the differences in the spectra of FMSZ and SZ at wavelengths below ~500 nm. MSZ absorbs rather strongly in the entire wavelength range because of its gray color. The same is true for FMSZ, but the aforementioned edge at 571 nm is still clearly visible.

The absorptions and the first derivative curves characterizing the reference compounds MnO, $MnO_2$, and FeO are not shown because the absorption spectra are much different from those of the catalyst samples. Other reference compounds were examined, $FeSO_4 \cdot 7H_2O$, $Fe_2(SO_4)_3 \cdot xH_2O$, and $MnSO_4 \cdot 6H_2O$, but no features were found to match those of the spectra of the catalysts.

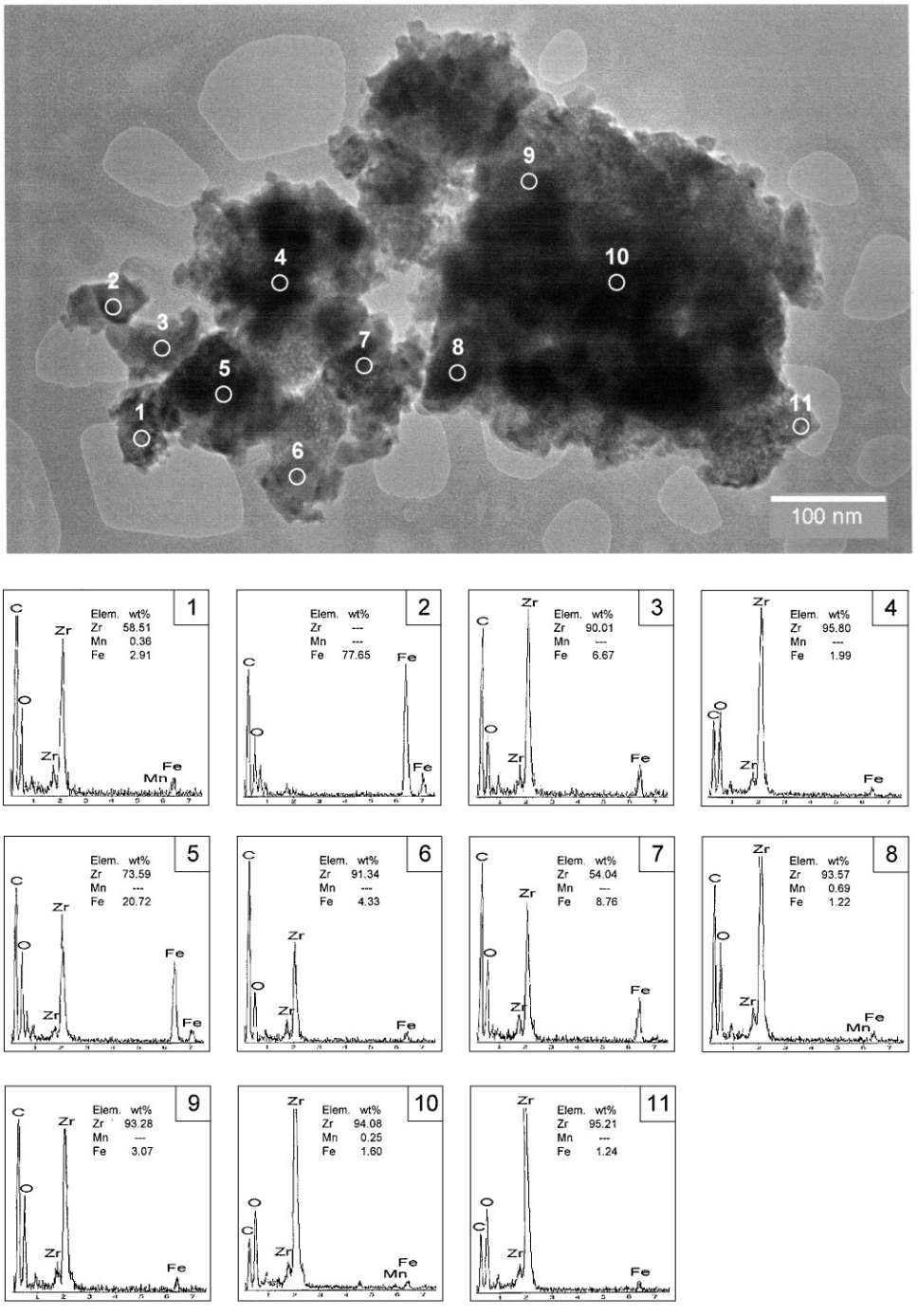


**FIG. 4.** Micrograph and EDX analysis of sample FMSZ.

*ESR Spectra*

The ESR spectra characterizing FMSZ, FSZ, and MSZ, measured in air with no sample pretreatment, are shown in Fig. 9. The spectrum of FSZ is characterized by one signal at $g = 4.3$ and a second, highly asymmetric, and broad signal at $g = 2.0$. Its amplitude was much lower than those of MSZ and FMSZ. The spectrum of MSZ exhibited only a broad signal with a g-factor of 2.0, with the intensity exceeding that of FMSZ. The FMSZ spectrum also shows a hyperfine splitting within the broad signal, with a g-factor of about 2. The doubly integrated intensities of the FMSZ and MSZ spectra were determined to be 9.1 and 18.3 (arbitrary units), respectively. Because the ESR signal characterizing FSZ is so broad, reliable integration could not be achieved.

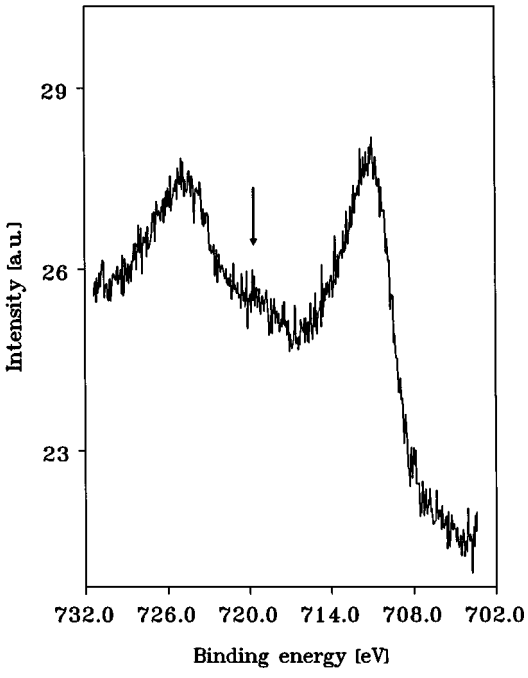


**FIG. 5.** XP spectrum of FMSZ showing the Fe2p emissions.

A reference sample consisting of a physical mixture of $Fe_2O_3$ and SZ (containing roughly 2 wt% Fe) was also investigated, its ESR spectrum (not shown) consisting essentially of a broad signal with a g-factor of about 2. The amplitude of the signal characterizing the mixture of $Fe_2O_3$ and SZ is 10 times higher than that of the signal characterizing FSZ.

The effect of vacuum pretreatment (at 200°C for 2 h) followed by the introduction of $O_2$ into the FMSZ sample is illustrated in Fig. 10. The hyperfine structure of the spectrum was barely affected relative to that of the unpretreated or evacuated sample, irrespective of whether the $O_2$ exposure and the ESR measurement were carried out at room temperature or at liquid $N_2$ temperature.

## DISCUSSION

### *Lack of Effect of Promoters on Structures of Bulk Zirconia and Sulfate Groups*

The Raman spectrum of each sample includes peaks at 146, 270, 316, 460, and 645 $cm^{-1}$ Fig. 6), consistent with literature data for sulfated zirconia (25, 26) and giving evidence of tetragonal zirconia. This conclusion is supported by XRD results indicating that the samples consisted predominantly of this zirconia phase. Evidently, the promoters do not change the bulk zirconia structure.

The 1034 $cm^{-1}$ peak in the Raman spectrum of each of the catalysts (Fig. 6) is characteristic of hydrated sulfate groups (26), and the lack of a significant change in the frequency of this peak upon addition of promoters shows that the promoters do not affect the sulfate groups significantly. The data are not sufficient for a full characterization of the sulfate group structures.

### *Evidence of Oxidation States of Zr, Fe, Mn, and S*

The data provide evidence of the oxidation states of several of the elements in the catalysts. For example, the XPS data indicate the presence of $Zr^{4+}$ in each sample, consistent with the presence of bulk $ZrO_2$ and confirming the Raman and XRD results. The XPS data also indicate the presence of $S^{6+}$, consistent with the Raman evidence of sulfate groups.

Furthermore, the XPS data provide evidence of the oxidation states of the promoter metals, as follows: The iron-containing samples (FSZ and FMSZ) are characterized by Fe2p emissions at 711.1 and 724.9 eV and a satellite at ~720 eV, which are indicative of $Fe^{3+}$ (19–21); no other iron species are recognizable in the XP spectra of these samples. The manganese-promoted sample (MSZ) is characterized by a weak peak at ~641 eV, which is likely indicative of $Mn^{2+}$. The XP spectrum of FMSZ lacks any clearly discernible peaks attributed to manganese, because of the low Mn concentration and because the Mn may not be located at the surface, as indicated by the ESR results.

### *Evidence of Dispersed $Fe_2O_3$ in Iron-Containing Catalysts*

The UV-vis spectra of the iron-containing samples (Fig. 8A) are not characterized by bands that would be indicative of isolated (nearly molecular) species such as were

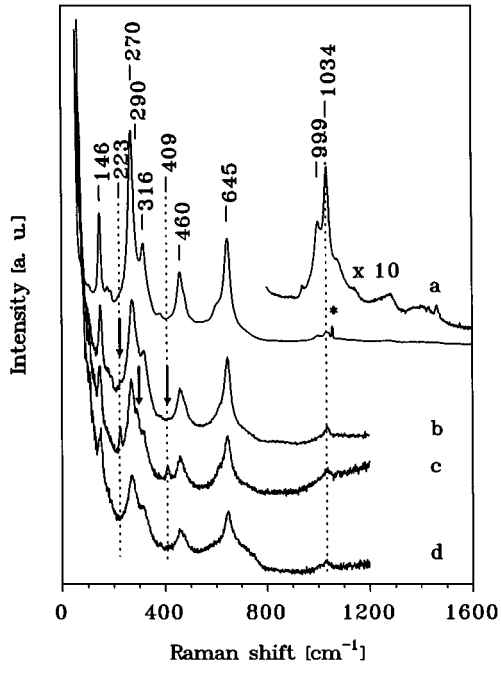


**FIG. 6.** Raman spectra of (a) SZ, (b) FSZ, (c) FMSZ, and (d) MSZ. (∗ indicates plasma lines of the laser).

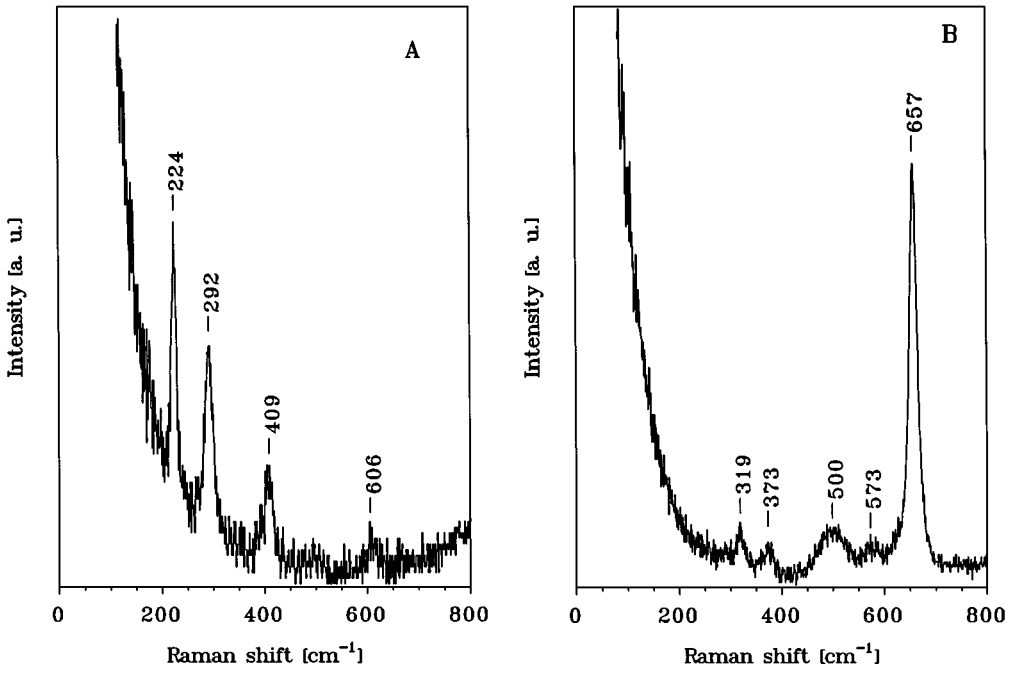


**FIG. 7.** Reference Raman spectra of (A) $Fe_2O_3$ and (B) MnO.

hypothesized by Benaissa *et al*. (11). Instead, the spectra of Fe-containing samples are characterized by edges at 571 nm that are indicative of optically stimulated electron transitions across the forbidden band gap in $Fe_2O_3$. The width of the band gap of $\alpha$-$Fe_2O_3$ (27) and that of colloidal $Fe_2O_3$ (28) have been reported to be 2.2 eV (564 nm). This value is very close to the absorption edges observed in this work for FSZ and FMSZ. The spectra are thus consistent with the Raman and XPS data and with particulate iron oxide on the surfaces of FSZ and FMSZ.

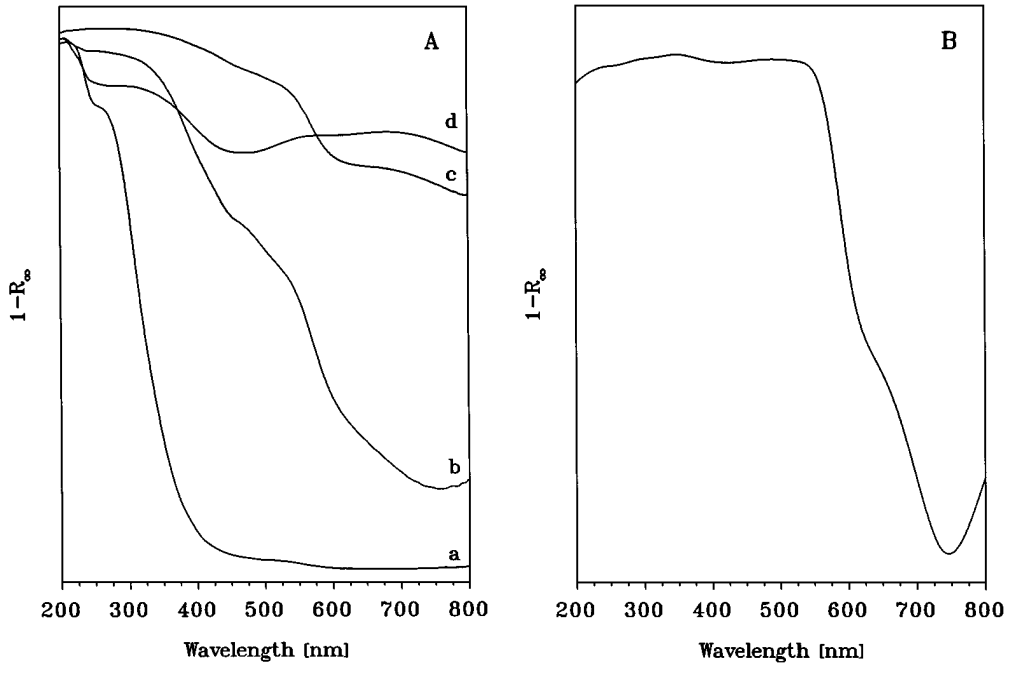


**FIG. 8.** UV-vis diffuse reflectance spectra of (A) catalyst samples (a) SZ, (b) FSZ, (c) FMSZ, and (d) MSZ, and (B) $Fe_2O_3$.

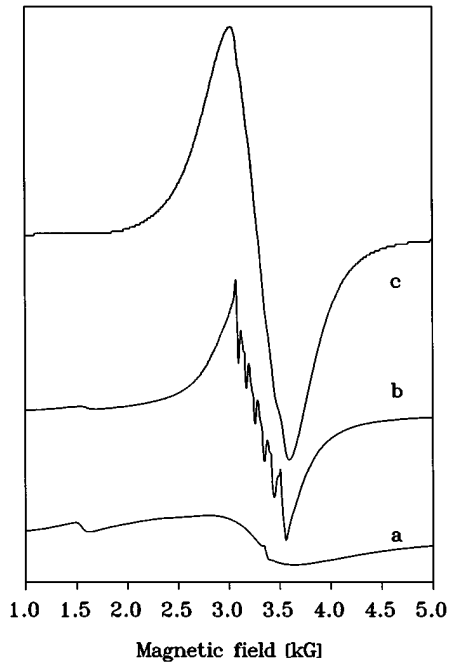


**FIG. 9.** ESR spectra of (a) FSZ, (b) FMSZ, and (c) MSZ.

The TEM data provide evidence of small clusters dispersed on the surfaces of the iron-containing catalysts and not the others (Fig. 2). Thus, we identify the dispersed species as $Fe_2O_3$ on the zirconia support. Typical dimensions of the supported iron oxide clusters are in the range 1–2 nm. The EDX spectra taken at various positions on the surfaces of the iron-containing catalysts FSZ (Fig. 3) and FMSZ (Fig. 4) confirm the presence of iron, but the spot sizes were not small enough to allow determinations of the compositions of the supported clusters.

The ESR spectrum of FSZ (spectrum a, Fig. 9) is characterized by a superposition of several signals indicative of different symmetries of structures around the $Fe^{3+}$ ions. Depending on the values of the fine structure parameters D and E and the symmetry of the site, trivalent iron can give rise to numerous resonances over a wide range of effective g values (29). The signal at $g = 4.3$ (30/7 signal) can be assigned to isolated $Fe^{3+}$ ions in cubic symmetry of strong rhombic distortion, $E/D = 1/3$ (29). Other signals, except for the sharp signal caused by a small number of free electrons, cannot be clearly separated from the broad line shape centered at approximately $g = 2.3$. These signals (for example, near $g = 3.2$) may be indicative of $Fe^{3+}$ ions having particular combinations of fine structure parameters in various lower symmetry environments (29). The $Fe^{3+}$ signal at $g = 2.3$ may be attributed to cubic $Fe^{3+}$, provided that the zero field splitting is small, or to antiferromagnetically coupled clusters (30). $Fe^{3+}$ ions in $\alpha$-$Fe_2O_3$ are coordinated by a distorted oxygen octahedron. In $\gamma$-$Fe_2O_3$, the $Fe^{3+}$ ions occupy octahedral and tetrahedral sites in a spinel structure; in small particles the local environment of the $Fe^{3+}$ ions may be differently distorted. We therefore infer that the ESR spectra of FSZ are consistent with the presence of small $Fe_2O_3$ particles, with some isolated $Fe^{3+}$ ions possibly being present as well.

The broad signal characterizing MSZ is probably caused by $Mn^{2+}$ centers in close proximity to each other, as the hyperfine structure is hardly visible, presumably because of dipole–dipole interactions. The differences in the signal intensities of the FSZ and MSZ samples can be explained by highly anisotropic transition probabilities in the case of large zero-field splitting parameters (31).

FMSZ shows the features of both $Fe^{3+}$ (as in FSZ) and $Mn^{2+}$. A striking observation is the appearance of the $Mn^{2+}$ hyperfine splitting of isolated ions in addition to the broad line that also appears in the spectrum of MSZ. The presence of isolated $Mn^{2+}$ ions in FMSZ may be simply explained by the low concentration of manganese in this sample. The hyperfine splitting was not affected by the exposure to $O_2$, which suggests that these $Mn^{2+}$ ions were not on the surface. The location of these sites remains unknown.

The EDX data show marked nonuniformities in the surface compositions (Figs. 3 and 4). These results are consistent with the inference that iron oxide clusters were dispersed nonuniformly on the surface of the zirconia. There is no correlation between the signals for Mn and those for Fe; and thus we are not able to draw any conclusions from the microscopic data regarding the possible association of the two promoter components in FMSZ.

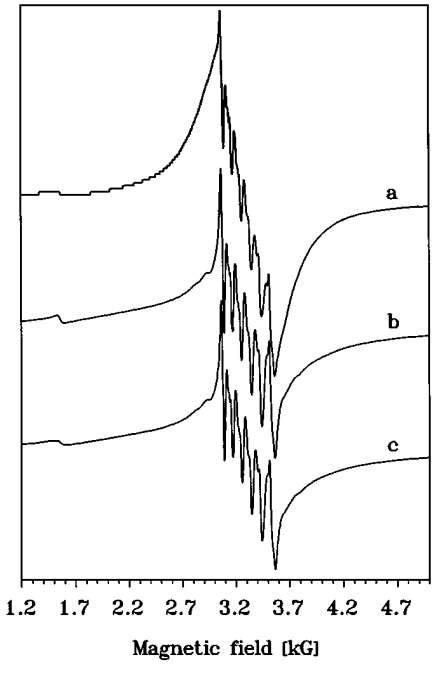


**FIG. 10.** Effect of vacuum pretreatment and subsequent exposure to $O_2$ on the ESR hyperfine splitting of $Mn^{2+}$ in FMSZ: (a) prior to pretreatment; (b) after evacuation at 200°C for 1 h; and (c) after exposure to $O_2$ at 25°C.

## SUMMARY OF STRUCTURAL CONCLUSIONS AND COMPARISON WITH LITERATURE

On the basis of the experimental results reported here, we infer that the tetragonal phase of $ZrO_2$ and the nature of the surface sulfate groups were essentially the same in the promoted samples FSZ, MSZ, and FMSZ as in the unpromoted SZ. The promoter elements were distributed nonuniformly in these catalysts. The data indicate the presence of supported $Fe_2O_3$ particles with typical dimensions of 1–2 nm in both FSZ and FMSZ. Isolated $Fe^{3+}$ ions, detected only by ESR, may also have been present in low concentrations. The coordination environment around the $Fe^{3+}$ ions in the $Fe_2O_3$ particles is presumably variably distorted, consistent with the fact that Tabora and Davis (10) did not observe Fe–Fe or Fe–Zr contributions in the EXAFS spectra characterizing their FMSZ. The small amounts of $Mn^{2+}$ in FMSZ seem to be present partly in oxide clusters (which allow dipole–dipole coupling), with isolated and inaccessible $Mn^{2+}$ ions also being present in still unknown locations.

The present results are consistent with the inference of Tabora and Davis (10) in that the iron is present in small clusters in FMSZ, and they are in contrast to the suggestion of Benaissa *et al*. (11) that iron and manganese were both dispersed at the atomic level on the zirconia surface in their samples. The apparent disagreement is not resolved; the possibility that the structures are sensitive to preparation conditions is not ruled out.

The present structural description of promoted SZ does not allow an interpretation of the promoter effects of iron and manganese oxides (6, 13–15). The experimental results do not provide any evidence of interactions between iron and manganese oxides, and the reported cooperative action of the two promoter oxides (12) still remains to be explained.

## ACKNOWLEDGMENTS

We thank Professor M. Che for valuable discussions and Dipl. Chem. B. Spliethoff for assistance with the electron microscopy. The international collaboration was made possible by the support of the Alexander von Humboldt-Stiftung and the Max-Planck-Gesellschaft. The work in California was supported in part by the University of California Energy Institute; that done in Munich was financially supported by the Deutsche Forschungsgemeinschaft (SFB 338), the Bayerische Forschungsverbund Katalyse FORKAT, and the Fonds der Chemischen Industrie.

## REFERENCES

1. Arata, K., *Adv. Catal.* **37**, 165 (1990).
2. Song, X., and Sayari, A., *Catal. Rev.-Sci. Eng.* **38**, 329 (1990).
3. Tanabe, K., Hattori, H., and Yamaguchi, T., *Crit. Rev. Surf. Chem.* **1**, 1 (1990).
4. Yamaguchi, T., *Appl. Catal.* **61**, 1 (1990).
5. Schüth, F., and Stichert, W., personal communication, March 1997.
6. Hsu, C.-Y., Heimbuch, C. R., Armes, C. T., and Gates, B. C., *Chem. Commun.*, 1645 (1992).
7. Kustov, L. M., Kazansky, V. B., Figueras, F., and Tichit, D., *J. Catal.* **150**, 143 (1994).
8. Yamaguchi, T., Jin, T., Ishida, T., and Tanabe, K., *Mat. Chem. Phys.* **17**, 3 (1987).
9. Bensitel, M., Saur, O., Lavalley, J.-C., and Morrow, B. A., *Mat. Chem. Phys.* **19**, 147 (1988).
10. Tabora, J. E., and Davis, R. J., *J. Chem. Soc. Faraday Trans.* **91**, 1825 (1995).
11. Benaissa, M., Santiesteban, J. G., Diaz, G., and Yacaman, M. J., *Surf. Sci. Lett.* **364**, L591 (1996).
12. Lange, F. C., Cheung, T.-K., and Gates, B. C., *Catal. Lett.* **41**, 95 (1996).
13. Cheung, T.-K., d'Itri, J. L., and Gates, B. C., *J. Catal.* **151**, 464 (1995).
14. Adeeva, V., de Haan, J. W., Jänchen, J., Lei, G. D., Schünemann, V., van de Ven, L. J. M., Sachtler, W. M. H., and van Santen, R. A., *J. Catal.* **151**, 364 (1995).
15. Coelho, M. A., Alvarez, W. E., Sikabwe, E. C., White, R. L., and Resasco, D. E., *Catal. Today* **28**, 415 (1996).
16. Knoll, P., Singer, R., and Kiefer, W., *Appl. Spectrosc.* **44**, 776 (1990).
17. Spielbauer, D., *Appl. Spectrosc.* **49**, 650 (1995).
18. Wagner, C. D., Riggs, W. M., Davis, L. E., Moulder, J. F., and Muilenberg, G. E., "Handbook of X-Ray-Photoelectron Spectroscopy," Perkin-Elmer Corp., Eden Prairie, MN, 1979.
19. Brundle, C. R., Chuang, T. J., and Wandelt, K., *Surf. Sci.* **68**, 459 (1977).
20. Muhler, M., Schlögl, R., and Ertl, G., *J. Catal.* **138**, 413 (1992).
21. Schedel-Niedrig, Th., Weiss, W., and Schlögl, R., *Phys. Rev. B* **52**, 17450 (1995).
22. Kwok, C.-K., and Aita, C. R., *J. Appl. Phys.* **66**, 2756 (1989).
23. Tench, A. J., and Pott, G. T., *Chem. Phys. Lett.* **26**, 590 (1974).
24. Klier, K., *Catal. Rev.* **1**, 207 (1968).
25. Spielbauer, D., Mekhemer, G. A. H., Bosch, E., and Knözinger, H., *Catal. Lett.* **36**, 59 (1996).
26. Spielbauer, D., Dissertation, Universität München, 1995.
27. Matsumoto, Y., *J. Solid State Chem.* **126**, 227 (1996).
28. Chatterjee, S., Sarkar, S., and Bhattacharyya, S. N., *Polymer* **34**, 1979 (1993).
29. Mabbs, F. E., and Collison, D., "Electron Paramagnetic Resonance of d Transition Metal Compounds," Elsevier, Amsterdam, 1992.
30. Dyrek, K., Sojka, Z., and Zabinski, W., *Mineral. Polon.* **26**, 9 (1995).
31. Yang, A.-S., and Cafney, R. Y., *Biophys. J.* **51**, 55 (1987).